Synthesis of Lumped and Distributed Networks for Impedance Matching of Complex Loads

ROBERT M. COTTEE AND WILLIAM T. JOINES, MEMBER, IEEE

***Abstract*—Numerically generated results based on existing theoretical restrictions are presented enabling the straight-forward synthesis of ladder type networks for matching a resistive source to a complex load. Transfer functions used in the synthesis allow increased bandwidths via tradeoffs with reflection coefficients. Both lumped and distributed networks are treated and are fully illustrated with practical examples including, in the distributed case, experimental verification.**

I. Introduction

THEORETICAL restrictions applying to networks matching a resistive source to a complex load have been well treated in the literature, in particular by Fano [1] in 1950, who extended early work by Bode [2] and more recent work by Youla [3] and Chan and Kuh [4]. Although a number of papers have appeared making use of this theory [5]–[9], its application in practice for all but the simplest of loads has been limited by computational difficulties. It is the purpose of this paper to formulate procedures and present results which overcome the above difficulties and lead readily to the solution of some common impedance matching problems.

The paper is organized in the following manner, Section II presents the integral gain-bandwidth restrictions of Fano as applicable to lumped ladder type matching networks. Section III is devoted to the synthesis of such networks and illustrates this by way of an example based on numerically generated curves of the integral restrictions of Section II. Section IV compliments Section III by treating the corresponding synthesis of distributed ladder type impedance matching networks suitable for microwave frequencies. A practical example in the form of a broadband microwave transistor amplifier illustrates the distributed-element synthesis procedure. Section V demonstrates the usefulness of these procedures by presenting experimental results for the amplifier design of Section IV.

II. Gain Bandwidth Restrictions

Fano has derived a complete set of integral gain-bandwidth restrictions, which form necessary and sufficient conditions for the realizability of matching networks terminated in an arbitrary load impedance. The derivation of these results is fully covered in Fano's original paper [1] and only the appropriate results will be given here.

Manuscript received August 11, 1976; revised February 6, 1978.
The authors are with the School of Engineering, Duke University, Durham, NC 27706.

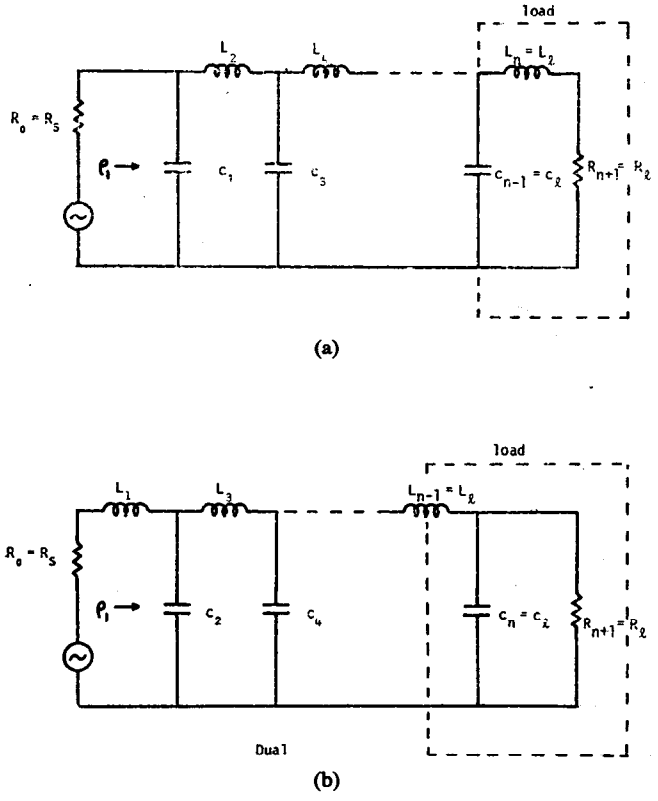

Fig. 1. Lumped element matching network and load.

For the three element load shown as part of the overall matching network of Fig. 1, the appropriate integral restrictions are as follows:

$$\int_0^\infty \ln \frac{1}{|\rho_1|}\, d\omega = \frac{\pi}{L_l} - \pi \sum_i p_{ri} \tag{1a}$$

$$\int_0^\infty \omega^2 \ln \frac{1}{|\rho_1|}\, d\omega = \frac{\pi}{L_l^3}\left(\frac{L_l}{C_l} - \frac{1}{3}\right) + \frac{\pi}{3}\sum_i p_{ri}^3 \tag{1b}$$

where ρ_1 is the input reflection coefficient to the matching network, ω is the normalized angular frequency, and P_{ri} are the zeros of ρ_1 in the right-half plane. Study of (1a) shows that the left-hand side, representing the area under the curve $\ln 1/|\rho_1|$ versus frequency, is fixed (apart from the $\Sigma_i P_{ri}$ term) by the value of the reactive element next to the load resistance. Similarly, (1b) shows the area under the curve $\omega^2 \ln 1/|\rho_1|$ versus frequency is fixed by the two reactive elements next to the load resistance. Both equations then represent gain-bandwidth type restrictions, with

0098-4094/79/0500-0316$00.75 ©1979 IEEE

the second equation being heavily weighted for higher frequencies. For the network under consideration maximization of the area under the curve $\ln 1/|\rho_1|$ versus frequency is achieved by setting $\Sigma_i P_{ri}$ equal to zero (see Fano [1] for a more complete discussion). It can be shown that the results for the dual circuit of Fig. 1(b) are identical to those of (1), except that L_l and C_l are interchanged.

III. Lumped Impedance Matching Network Synthesis

A. The Transfer Function and Its Parameters

In this section ladder type impedance matching networks of the form shown in Fig. 1(b) will be synthesized using procedures described by Matthaei [10] and the integral restrictions of (1).

Fig. 2 shows a typical response for the networks to be synthesized. The transfer function for this response is derived from the conventional Chebyshev low-pass filter transfer function given by

$$\frac{P_{\text{avail}}}{P_{\text{out}}} = \frac{1}{|t'|^2} = \begin{cases} 1+\epsilon \cosh^2 (n' \cosh^{-1} \omega'), & \text{for } 1 \leqslant \omega' \leqslant \infty \\ \omega+\epsilon \cos^2 (n' \cos^{-1} \omega'), & \text{for } 0 \leqslant \omega' \leqslant 1 \end{cases} \tag{2}$$

where ω' is the sinusoidal frequency variable normalized for unity cutoff frequency, n' is the number of reactive elements in the network, and ϵ is a parameter controlling the amplitude of the ripple. The appropriate transfer function for the response of Fig. 2 is obtained by using the change of frequency variable

$$\omega' = \frac{\omega^2 - \omega_0^2}{A} \tag{3}$$

where

$$A = \frac{\omega_b^2 - \omega_a^2}{2} \tag{4}$$

and

$$\omega_0 = \sqrt{\frac{\omega_a^2 + \omega_b^2}{2}} \tag{5}$$

is the frequency in the response of Fig. 2 corresponding to $\omega' = 0$ in the conventional Chebyshev low-pass filter characteristic. In addition, the mean operating frequency ω_m is given by

$$\omega_m = \frac{\omega_a + \omega_b}{2} \tag{6}$$

and is scaled so that $\omega_m = 1$.

The relative bandwidth w is defined as

$$w = \frac{\omega_b - \omega_a}{\omega_m} = \omega_b - \omega_a \tag{7}$$

where

$$\omega_a = 1 - \frac{w}{2} \tag{8}$$

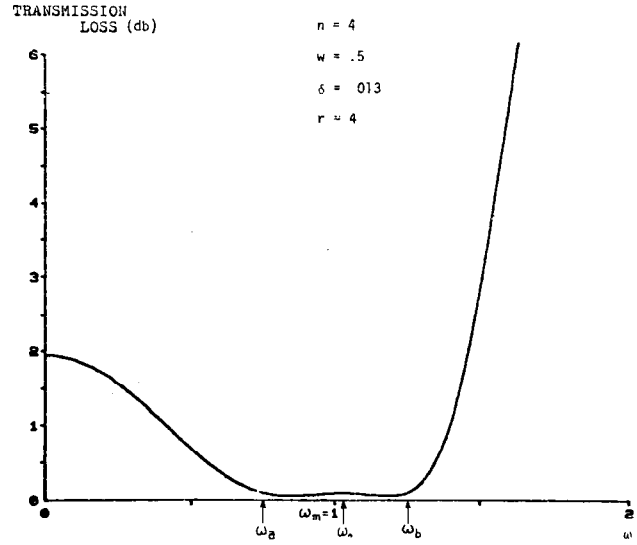

Fig. 2. Lumped element network transfer function response.

and

$$\omega_b = 1 + \frac{w}{2}. \tag{9}$$

Applying the change of frequency variable of (3) to (2) leads to the following transfer function:

$$\frac{P_{\text{avail}}}{P_{\text{out}}} = \frac{1}{|t|^2} = 1 + \delta + \epsilon \cosh^2 \left[\frac{n}{2} \cosh^{-1} \frac{(\omega^2 - \omega_0^2)}{A} \right] \tag{10a}$$

which applies in the "stop" bands $0 \leqslant \omega \leqslant \omega_a$ and $\omega_b \leqslant \omega \leqslant \infty$. In the operating band $\omega_a \leqslant \omega \leqslant \omega_b$,

$$\frac{P_{\text{avail}}}{P_{\text{out}}} = \frac{1}{|t|^2} = 1 + \delta + \epsilon \cos^2 \left[\frac{n}{2} \cos^{-1} \frac{(\omega^2 - \omega_0^2)}{A} \right]. \tag{10b}$$

Two points need clarification with respect to the transfer function in (10). First, the conventional low-pass Chebyshev response for a filter with n' reactive elements maps into a response characterized by a filter having $n = 2n'$ reactive elements. For example, the response of Fig. 2 corresponds to an $n = 4$ reactive-element design. The corresponding conventional low-pass filter would have $n' = 2$ reactive elements. Second, an extra parameter δ has been introduced to ensure that the function $\ln 1/|\rho_1|$ in the integral gain-bandwidth restrictions of (1) does not go to infinity at any real frequencies. This point is illustrated in Fig. 3 where $\ln 1/|\rho_1|$ has been plotted as a function of frequency for the same parameters as were used in Fig. 2, except that δ has now been set to zero. As pointed out by Fano [1] this type of characteristic results in an unnecessary waste of the area represented by the integrals of (1).

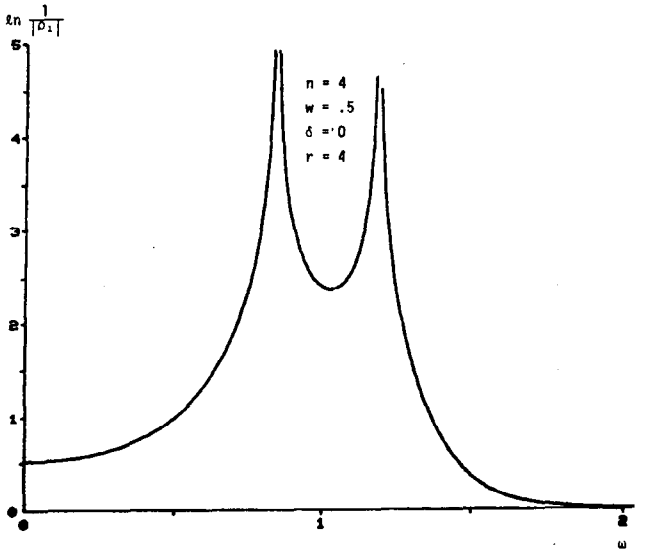

Fig. 3. $\ln 1/|\rho_1|$ vs ω for lumped element network with $\delta=0$.

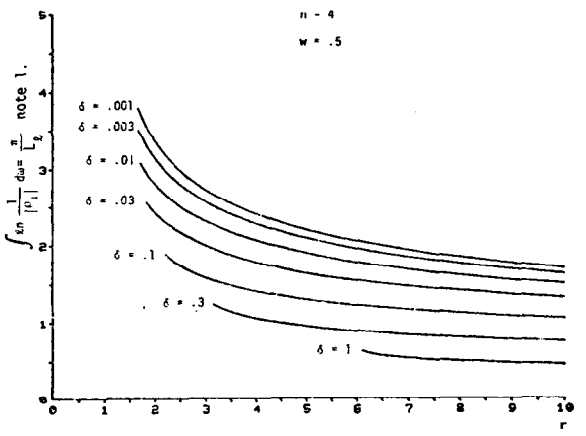

Fig. 4. Lumped network integral restrictions. Note: this equality applies for the network of Fig. 1(a). For the network of Fig. 1(b) interchange L_l and C_l.

B. Poles and Zeros

The synthesis procedure to follow later in this section requires that the poles and zeros of the reflection coefficient ρ_1 be evaluated. As a first step, the poles of $|\rho_1'|^2$ are evaluated for the conventional Chebyshev low-pass transfer function as [1]

$$p_p' = \begin{cases} \sinh\left[\pm a \pm j\dfrac{\pi}{n'}\left(m+\dfrac{1}{2}\right)\right], & n' \text{ even} \\ \sinh\left[\pm a \pm j\dfrac{\pi}{n'}m\right], & n' \text{ odd} \end{cases} \tag{11}$$

where m is an integer or zero, and a and b are defined by

$$\sinh^2 n'b = \frac{\delta}{\epsilon} \tag{12a}$$

and

$$\sinh^2 n'a = \frac{1+\delta}{\epsilon}. \tag{12b}$$

The zeros are given by the same expression in which b is substituted for a.

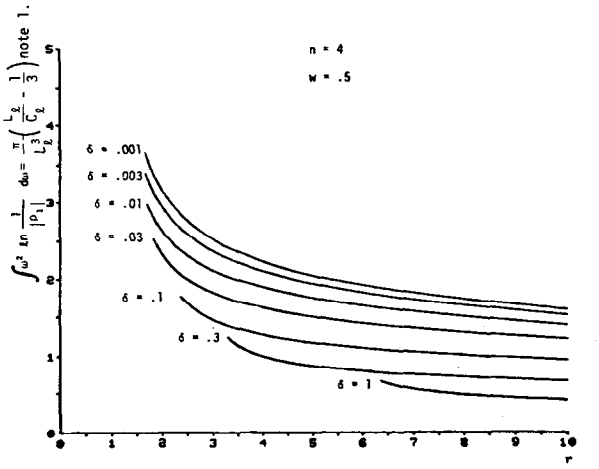

Fig. 5. Lumped network integral restrictions. Note: this equality applies for the network of Fig. 1(a). For the network of Fig. 1(b) interchange L_l and C_l.

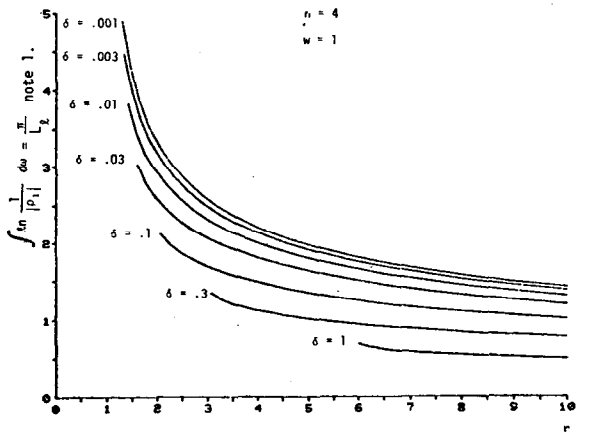

Fig. 6. Lumped network integral restrictions.

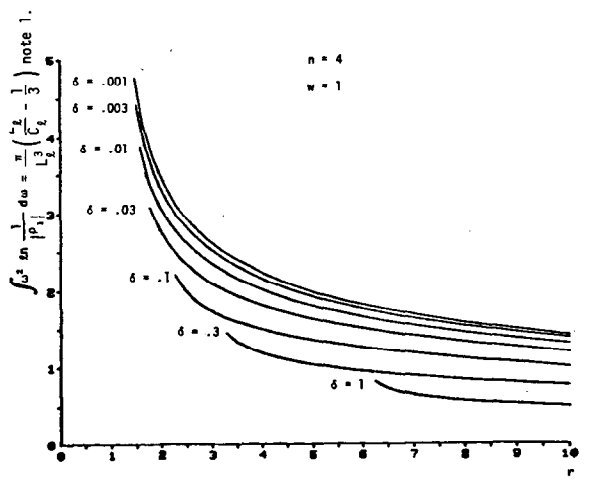

Fig. 7. Lumped network integral restrictions.

The poles and zeros of ρ_1 for the mapped transfer function are obtained from the poles and zeros of (11) by using

$$p' = -j\frac{(p^2+\omega_0^2)}{A} \tag{13}$$

obtained by replacing ω^1 by p'/j and ω by p/j in (3). In

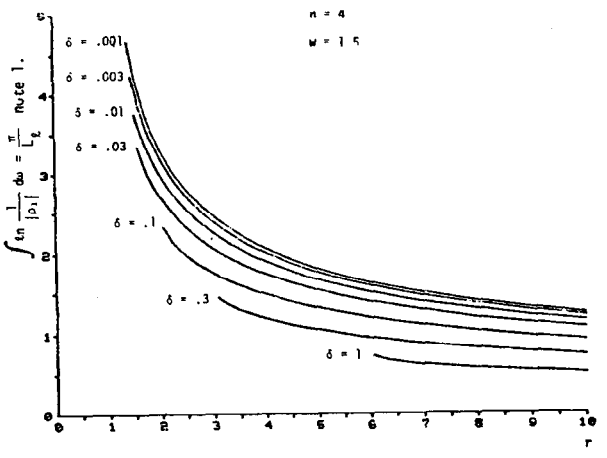

Fig. 8. Lumped network integral restrictions.

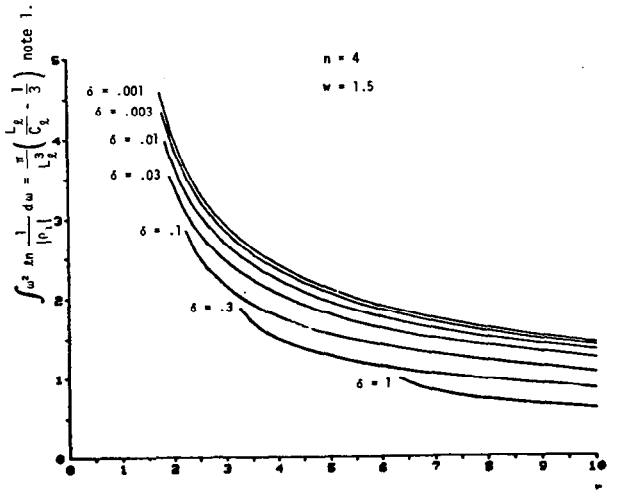

Fig. 9. Lumped network integral restrictions.

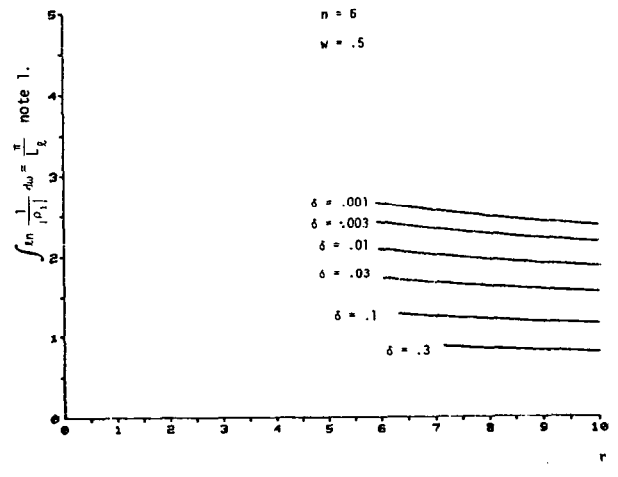

Fig. 10. Lumped network integral restrictions.

using (13), it should be noted that the poles of ρ_1 are necessarily those poles of $\rho_1(p)\rho_1(-p)$ which lie in the left-half plane. That is, in (11) "a" must be taken with the negative sign. The zeros of ρ_1, on the contrary, can be located anywhere in the complex plane. As pointed out earlier, however, the area represented by (1) is a maximum

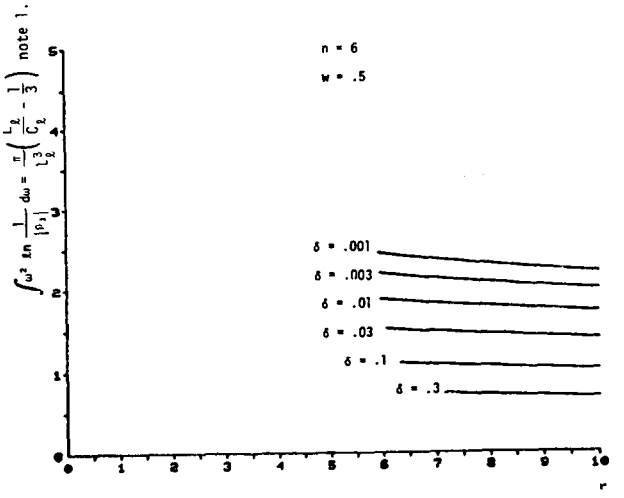

Fig. 11. Lumped network integral restrictions.

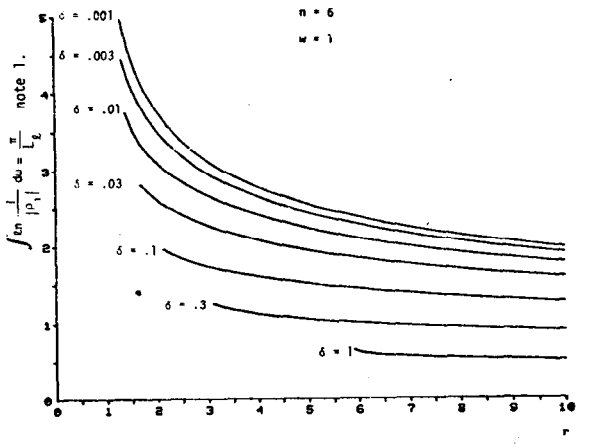

Fig. 12. Lumped network integral restrictions.

when all the zeros of ρ_1 are chosen to be in the left-half plane.

C. *Evaluation of the Gain-Bandwidth Integrals*

Using the expression

$$\ln \frac{1}{|\rho_1|} = \ln \sqrt{\frac{1+\delta+\epsilon \cosh^2\left[\frac{n}{2}\cosh^{-1}\frac{(\omega^2-\omega_0^2)}{A}\right]}{\delta+\epsilon\cosh^2\left[\frac{n}{2}\cosh^{-1}\frac{(\omega^2-\omega_0^2)}{A}\right]}} \tag{14a}$$

in the stopband, and

$$\ln \frac{1}{|\rho_1|} = \ln \sqrt{\frac{1+\delta+\epsilon \cos^2\left[\frac{n}{2}\cos^{-1}\frac{(\omega^2-\omega_0^2)}{A}\right]}{\delta+\epsilon\cos^2\left[\frac{n}{2}\cos^{-1}\frac{(\omega^2-\omega_0^2)}{A}\right]}} \tag{14b}$$

in the passband, the integrals of (1) have been evaluated numerically using the Gaussian method, and the results are presented in graphical form in Figs. 4–15. The in-

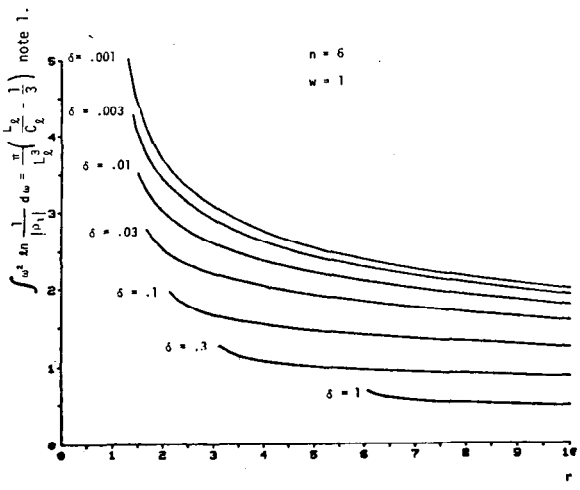

Fig. 13. Lumped network integral restrictions.

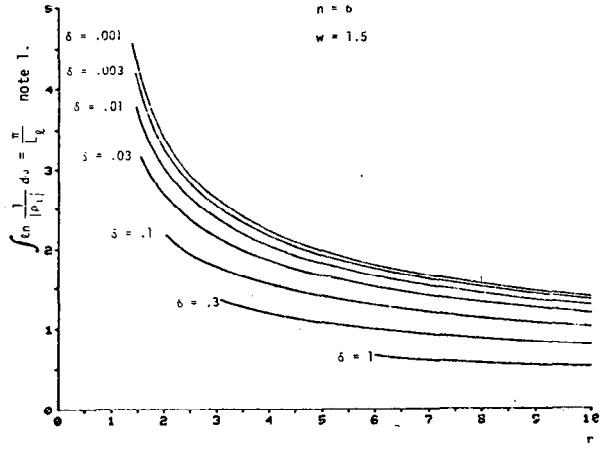

Fig. 14. Lumped network integral restrictions.

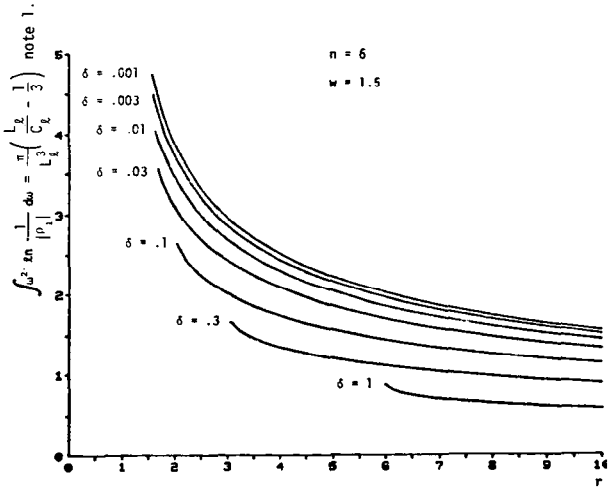

Fig. 15. Lumped network integral restrictions.

tegrals are plotted as a function of r, with δ as a parameter. Note that ϵ does not appear explicitly in these graphs because ϵ, δ, and the termination ratio r are not independent. The equation relating these three parameters is derived from (10a) using the condition that at $\omega=0$ (or DC) the power loss ratio is given by

$$\frac{1}{|t_{DC}|^2}=\frac{(r+1)^2}{4r}$$
$$=1+\delta+\epsilon\cosh^2\frac{n}{2}\left[\cosh^{-1}\left(\frac{\omega_0^2}{A}\right)\right]. \qquad (15)$$

It should be noted here that Figs. 4–15 could equally well have been obtained without numerical integration by using standard synthesis methods as has been done for example in producing the tables of [10]. The reason for using the integral approach is that it allows the restrictions to be visualized (e.g., as the area under Fig. 3) enabling suitable transfer functions to be chosen. This in fact was the motivation for the introduction of the mapping of (3) and of the parameter δ.

This completes the prerequisites for the synthesis, and an example follows to illustrate the procedures involved in a practical design.

D. Numerical Example of a Practical Matching Network

As an example, suppose that it is required to match the load shown in Fig. 16(a) to 50 Ω over the frequency band from 75–125 MHz. In addition, suppose that the maximum allowable insertion loss within this band is 0.1dB.

The mean frequency and relative bandwidth of the frequency response are calculated immediately as

$$\omega_m=\frac{75+125}{2}=100\text{ MHz}$$

and

$$w=\frac{125-75}{100}=0.5.$$

The normalized lower and upper band edges from (8) and (9) are then

$$\omega_a=1-\frac{0.5}{2}=0.75$$

and

$$\omega_b=1+\frac{0.5}{2}=1.25$$

and the frequency ω_0 is given from (5) as

$$\omega_0=\sqrt{\frac{0.75^2+1.25^2}{2}}=1.031.$$

Finally, the parameter A is computed from (4) as

$$A=\frac{1.25^2-0.75^2}{2}=0.5.$$

Using the arithmetic mean frequency of 100 MHz, the normalized load circuit is computed and is shown in Fig. 16(b).

From the normalized inductance and capacitance, the

integrals of (1) can now be evaluated, yielding

$$\int_0^\infty \ln \frac{1}{|\rho_1|}\, d\omega = \frac{\pi}{C_l} = \frac{\pi}{1.571} = 2.00 \tag{16a}$$

and

$$\int_0^\infty \omega^2 \ln \frac{1}{|\rho_1|}\, d\omega = \frac{\pi}{C_l^3}\left(\frac{C_l}{L_l} - \frac{1}{3}\right)$$

$$= \frac{\pi}{(0.5\pi)^3}\left(\frac{0.5\pi}{0.1\pi} - \frac{1}{3}\right) = 3.78. \tag{16b}$$

Referring to the numerically generated integrals for $n=4$ and $w=0.5$ of Fig. 4, the value $\delta=0.013$ is interpolated from the graph using the result from (16a) above and the termination ratio $r=4$. Referring now to Fig. 5, again by interpolation the value of the second integral for $\delta=0.013$ and $r=4$ is read as 1.82. This value is seen to be less than the upper limit set by the result from (16b), thus satisfying the second integral restriction. (The restriction of (16b) need only be "less than or equal to," since inductance can be physically added later to make up the required load inductance.)

Finally, we check to see that the maximum insertion loss requirement within the passband is satisfied. Evaluating ϵ from (15) using $r=4$, $n=4$, $\delta=0.013$, $\omega_0=1.031$, and $A=0.5$ gives $\epsilon=0.008503$, and the maximum insertion loss in the passband is then

$$L_{A\,\max} = 10 \log (1+\delta+\epsilon) = 0.09240 \text{ dB}.$$

This value is seen to be less than the original specification, and so the choice of $n=4$ is suitable. The expected frequency response with these parameters substituted into (10) is shown in Fig. 2.

Having satisfied the specification, the first step in the synthesis is to compute the poles and zeros of ρ_1' for the conventional Chebyshev low-pass filter. From (12), a and b are computed, respectively, as 1.543 and 0.5196, and from (11), the poles and zeros of $|\rho_1'|^2$ are computed as

$$p_{pi}' = \pm 1.579 \pm j1.730$$

and

$$p_{0i}' = \pm 0.3838 \pm j0.8047.$$

The poles and zeros for the corresponding mapped function are now obtained from the poles and zeros just computed using (13) as

$$p = -\omega_0^2 + jAp'$$

yielding

$$p_{pi} = 1.443 \exp(\pm j4.518), 0.9022 \exp(\pm 4.050)$$

and

$$p_{0i} = 1.216 \exp(\pm j4.647), 0.8294 \exp(\pm j4.571).$$

Utilizing left-half plane poles only, the expression for ρ_1

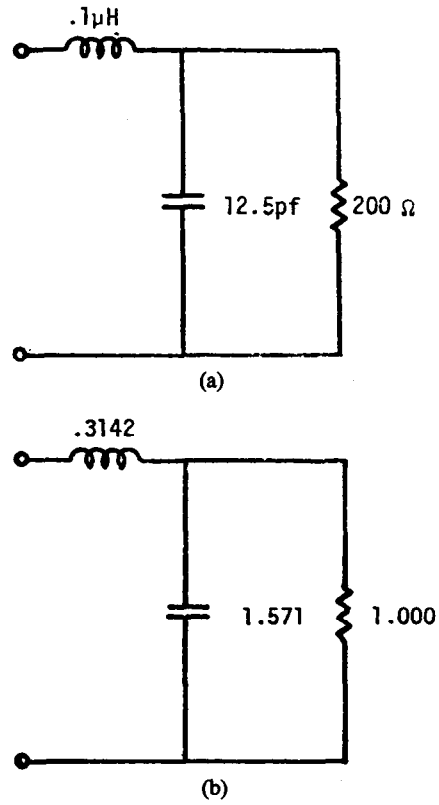

Fig. 16. Lumped element load. (a) Denormalized. (b) Normalized.

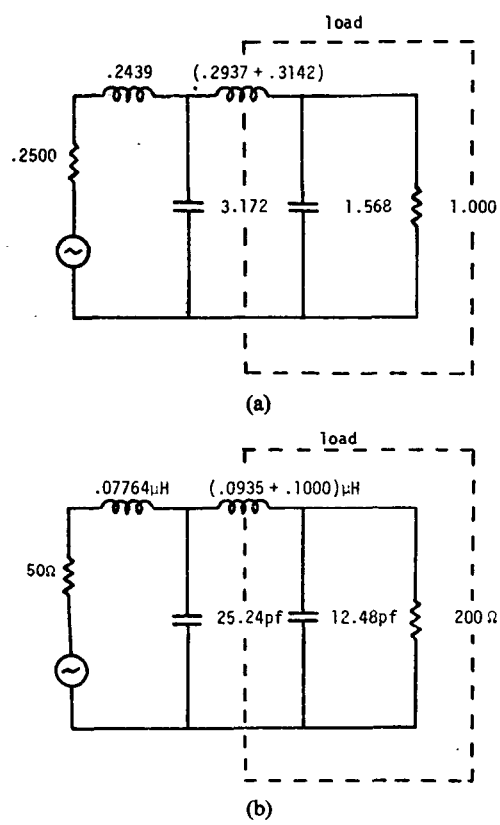

Fig. 17. Synthesized lumped element matching network. (a) Normalized. (b) Denormalized.

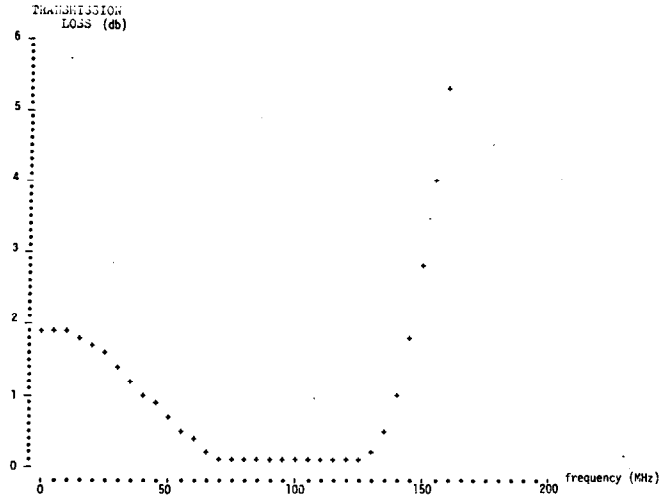

Fig. 18. Computer analysis plot of synthesized lumped element circuit.

can be written as

$$\rho_1(p)=\frac{(p-1.216e^{j4.647})(p-1.216e^{-j4.647})(p-0.8294e^{j4.571})(p-0.8294e^{-j4.571})}{(p-1.443e^{j4.518})(p-1.443e^{-j4.518})(p-0.9022e^{j4.050})(p-0.9022e^{-j4.050})}$$
$$=\frac{(p^2+.1589p+1.479)(p^2+0.2338p+0.6879)}{(p^2+.5575p+2.082)(p^2+1.110p+0.8140)}=\frac{p^4+.3927p^3+2.204p^2+.4551p+1.017}{p^4+1.668p^3+3.515p^2+2.765p+1.695}.$$

The input impedance of the network is computed as

$$z(p)=\frac{1-\rho_1}{1+\rho_1}=\frac{0.6377p^3+0.6555p^2+1.155p+0.3390}{p^4+1.030p^3+2.860p^2+1.610p+1.356}$$

and the elements of the network can now be obtained through continued fraction expansion of $y(p)$, yielding the circuit as shown in Fig. 17. A frequency response plot obtained from a computer network analysis program is shown in Fig. 18. Comparison of this figure with the original transfer function plot of Fig. 2 shows the excellent agreement obtainable.

IV. Distributed Impedance Matching Network Synthesis

A. The Transfer Function and Its Parameters

In this section distributed impedance matching networks of the types shown in Fig. 19 will be synthesized using procedures described by Matthaei [11], and the integral restrictions of (1) scaled appropriately to account for the distributed nature of the network.

As was the case in the previous section, the starting point for this synthesis is the conventional Chebyshev low-pass filter transfer function of (2). Fig. 20 shows a typical transfer function characteristic for the distributed circuit of Fig. 19. In order to map the Chebyshev low-pass characteristic into that of Fig. 20, it is necessary that certain requirements be met. The first requirement is to account for the fundamentally periodic nature of the distributed circuit elements by using the mapping

$$\omega=\tan\theta \tag{17}$$

first introduced by Richards [12]. The second requirement is to account for the finite out-of-band attenuation (as opposed to infinite attenuation for the low-pass Chebyshev case) by using another mapping of the form [11]

$$\omega'=A\left(\frac{\omega^2-\omega_0^2}{\omega^2+1}\right) \tag{18}$$

where A is a constant, and $\theta_0=\tan^{-1}\omega_0$ is the electrical length corresponding to $\omega'=0$ for the conventional Chebyshev low-pass filter response.

In addition to the above mappings, some further relationships are required to define the frequency response. The mean operating electrical length θ_m is given by

$$\theta_m=\frac{\theta_a+\theta_b}{2}=\frac{2\pi l}{\lambda_m} \tag{19}$$

and the relative bandwidth w is defined as

$$w=\frac{\theta_b-\theta_a}{\theta_m} \tag{20}$$

where

$$\theta_a=\theta_m\left(1-\frac{w}{2}\right) \tag{21}$$

and

$$\theta_b=\theta_m\left(1+\frac{w}{2}\right). \tag{22}$$

Solving for A by inserting (17) into (18) and using the fact that $\omega'=1$ when $\theta=\theta_b$ yields

$$A=\frac{1+\tan^2\theta_b}{\tan^2\theta_b-\tan^2\theta_0}. \tag{23}$$

The parameter $\tan\theta_0$ is determined by using (17), (18), and (23), together with the fact that $\omega'=-1$ when $\theta=\theta_a$, yielding

$$\tan\theta_0=\sqrt{\frac{(\tan\theta_b)^2\left[1+(\tan\theta_a)^2\right]+(\tan\theta_a)^2\left[1+(\tan\theta_b)^2\right]}{2+(\tan\theta_a)^2+(\tan\theta_b)^2}}. \tag{24}$$

One further parameter K will be used to define the maximum out-of-band reflection coefficient magnitude. The electrical lengths at which these maxima occur correspond to $\theta=m\pi/2$ or $\omega=\infty$. From (18), this corresponds to $\omega'=A$, and using this in (2) together with the fact that

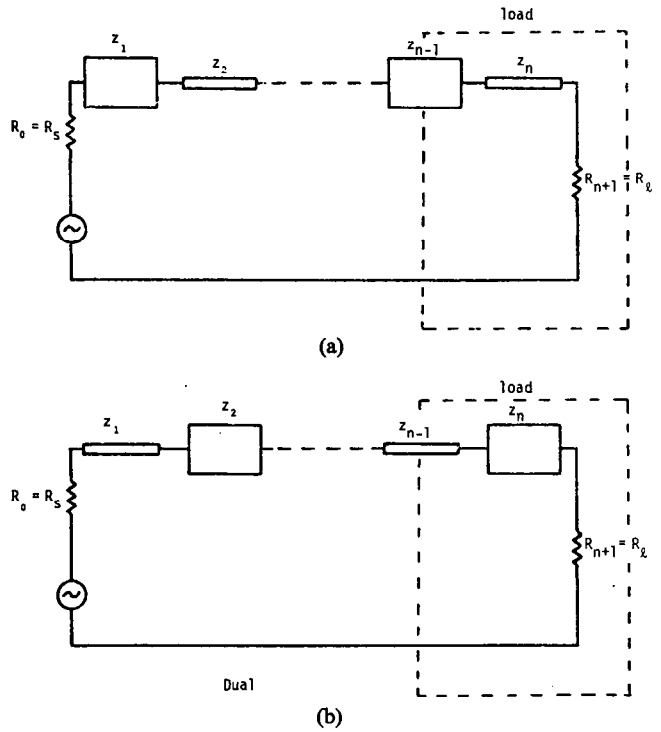

Fig. 19. Distributed element matching network and load.

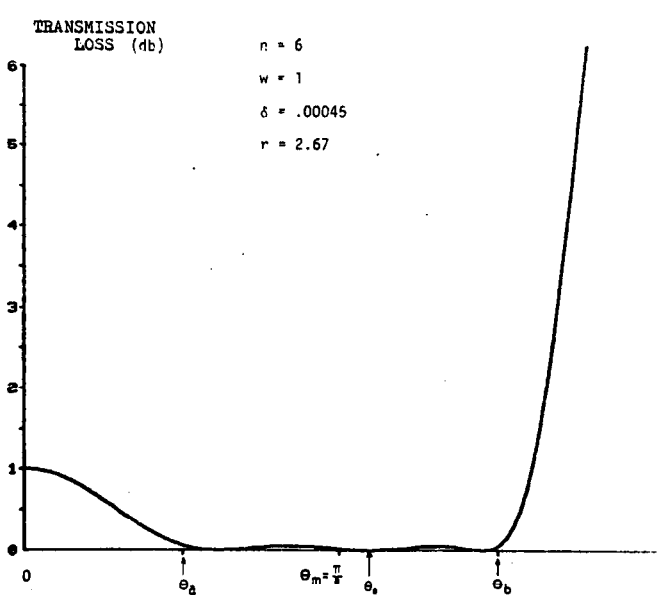

Fig. 20. Distributed element network transfer function response.

$|\rho_1|^2 = 1 - |t|^2$, results in the following expression for K,

$$K = |\rho_1|_{\omega=\infty} = \sqrt{\frac{\delta + \epsilon \cosh^2\left(\frac{n}{2}\cosh^{-1} A\right)}{1 + \delta + \epsilon \cosh^2\left(\frac{n}{2}\cosh^{-1} A\right)}}. \quad (25)$$

Applying the change of frequency variable of (17) and (18) to the conventional Chebyshev low-pass filter transfer function of (2), leads to the following transfer function

$$\frac{P_{\text{avail}}}{P_{\text{out}}} = \frac{1}{|t|^2} = 1 + \delta + \epsilon \cdot \cosh^2\left\{\frac{n}{2}\cosh^{-1}\left[A\frac{(\tan\theta)^2 - (\tan\theta_0)^2}{(\tan\theta)^2 + 1}\right]\right\} \quad (26a)$$

which applies in the "stop" bands $0 \leqslant \theta \leqslant \theta_a$ and $\theta_b \leqslant \theta \leqslant \pi/2$. In the operating band $\theta_a \leqslant \theta \leqslant \theta_b$

$$\frac{P_{\text{avail}}}{P_{\text{out}}} = \frac{1}{|t|^2} = 1 + \delta + \epsilon \cdot \cos^2\left\{\frac{n}{2}\cos^{-1}\left[A\frac{(\tan\theta)^2 - (\tan\theta_0)^2}{(\tan\theta)^2 + 1}\right]\right\}. \quad (26b)$$

B. Poles and Zeros

As for the lumped element case, the first step in the synthesis is to obtain the poles and zeros of $|\rho_1|^2$ for the conventional Chebyshev low-pass filter. Next, the poles and zeros of ρ_1 for the mapped transfer function are evaluated using the following equation, obtained from (18) by replacing ω' by p'/j and ω by p/j,

$$p' = jA\frac{p^2 + \omega_0^2}{p^2 - 1}. \quad (27)$$

C. Evaluation of the Gain-Bandwidth Integrals

The synthesis procedures to follow yield an all distributed element network characterized by harmonic passbands extending to infinity on the frequency scale. This would appear to preclude evaluation of the integrals in the restrictions of Section II. However, by replacing the load section of such a network by an equivalent lumped element load, the higher order passbands are attenuated resulting in a truncated frequency response which can be approximated by the fundamental passband only of the transfer function of (26). The accuracy of such an approximation depends on the fundamental passband remaining substantially unchanged, and on the degree to which the harmonic passbands are attenuated. This approach allows the integral restrictions of Section II to be applied for a lumped element load and a distributed element matching network. (For distributed element loads one is referred to Tucker [8] where the integrals have been transformed to the Richards domain. While results are not extensive, the approach is potentially more accurate and does not require the approximations made here.)

With this as a basis, the integrals have again been evaluated numerically by integrating the appropriate distributed function over the fundamental passband, i.e., for θ in the range of 0 to $\pi/2$. Using (19) with θ_m chosen as $\theta_m = \pi/8$ (a compromise between impractical line impedances for $\theta_m \ll \pi/8$ and a reduced gain bandwidth for $\theta_m \gg \pi/8$), the integral restrictions can be written as

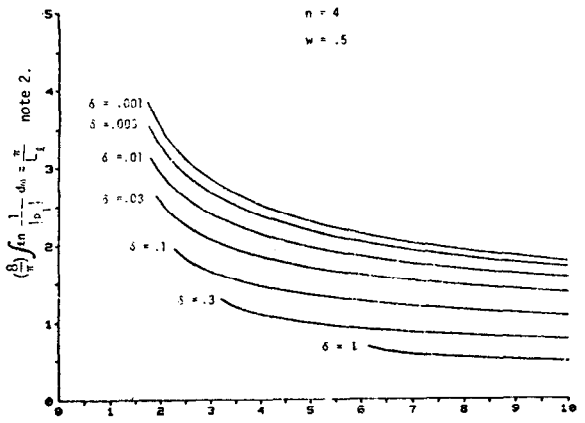

Fig. 21. Distributed network integral restrictions. Note: this equality applies for the network of Fig. 19(a) where L_l and C_l constitute a lumped element equivalent of the load shown. For the network of Fig. 19(b) interchange L_l and C_l.

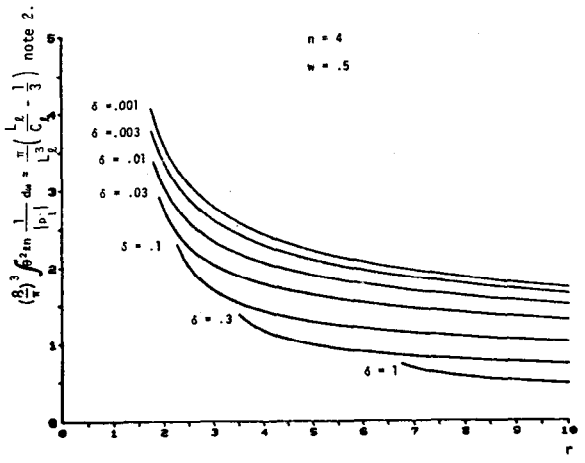

Fig. 22. Distributed network integral restrictions. Note: this equality applies for the network of Fig. 19(a) where L_l and C_l constitute a lumped element equivalent of the load shown. For the network of Fig. 19(b) interchange L_l and C_l.

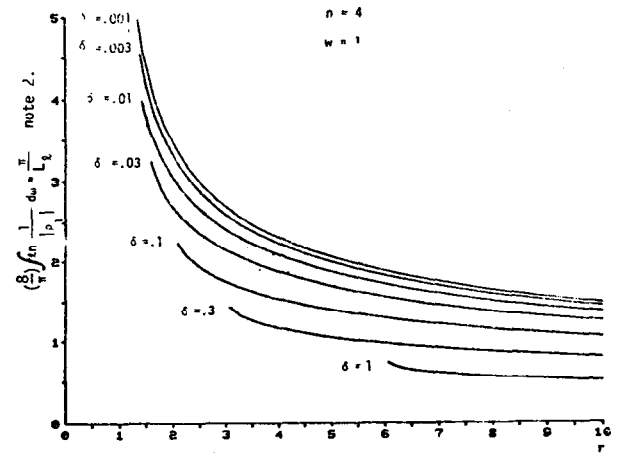

Fig. 23. Distributed network integral restrictions.

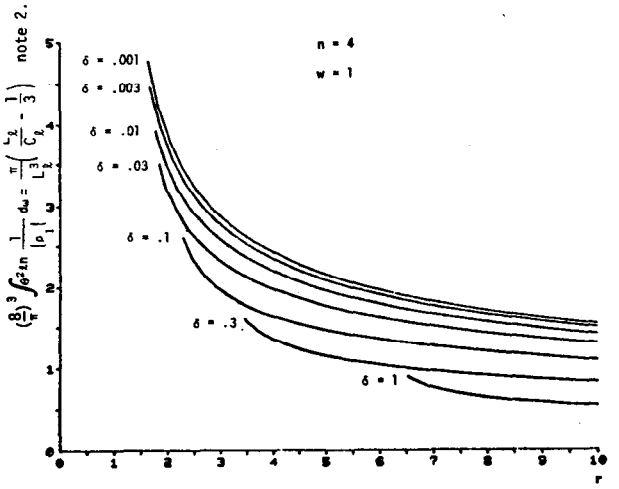

Fig. 24. Distributed network integral restrictions.

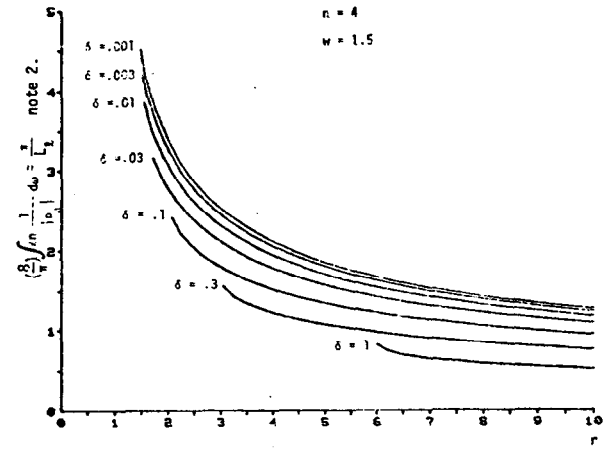

Fig. 25. Distributed network integral restrictions.

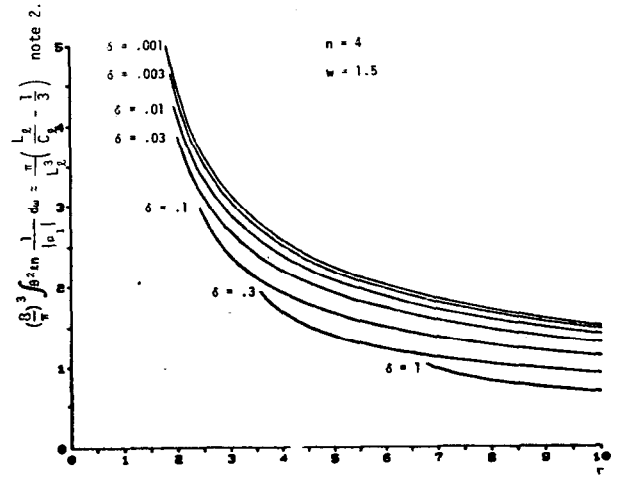

Fig. 26. Distributed network integral restrictions.

follows:

$$\left(\frac{8}{\pi}\right)\int_0^{\pi/2} \ln \frac{1}{|\rho_1(\theta)|}\, d\theta = \frac{\pi}{C_l} \tag{28a}$$

and

$$\left(\frac{8}{\pi}\right)^3\int_0^{\pi/2} \theta^2 \ln \frac{1}{|\rho_1(\theta)|}\, d\theta = \frac{\pi}{C_l^3}\left(\frac{C_l}{L_l} - \frac{1}{3}\right). \tag{28b}$$

Numerical integration of these equations, using the function $\ln 1/|\rho_1(\theta)|$ from (26a) and (26b) together with the

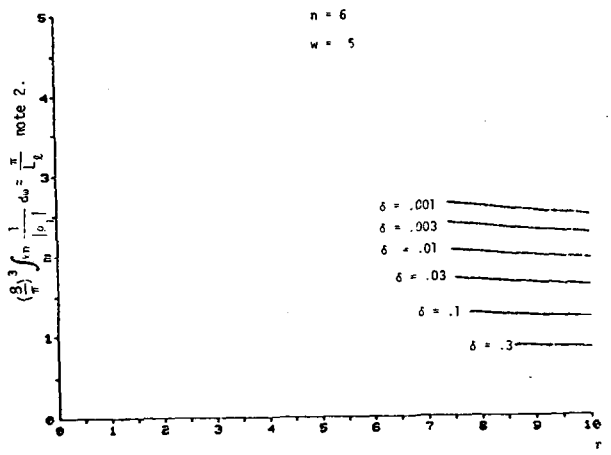

Fig. 27. Distributed network integral restrictions.

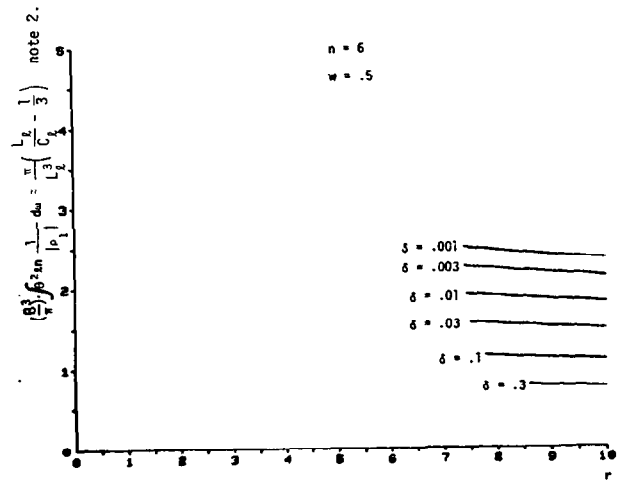

Fig. 28. Distributed network integral restrictions.

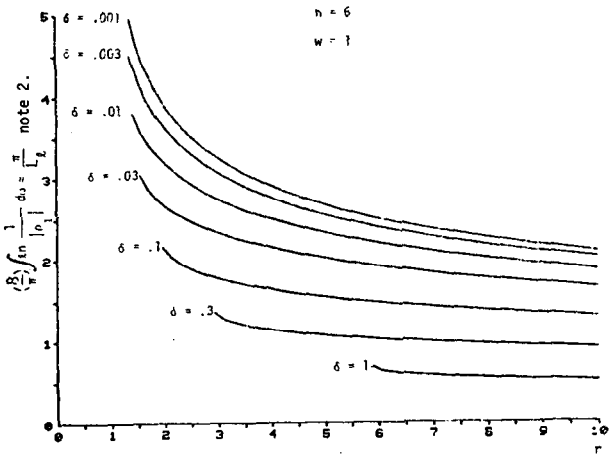

Fig. 29. Distributed network integral restrictions.

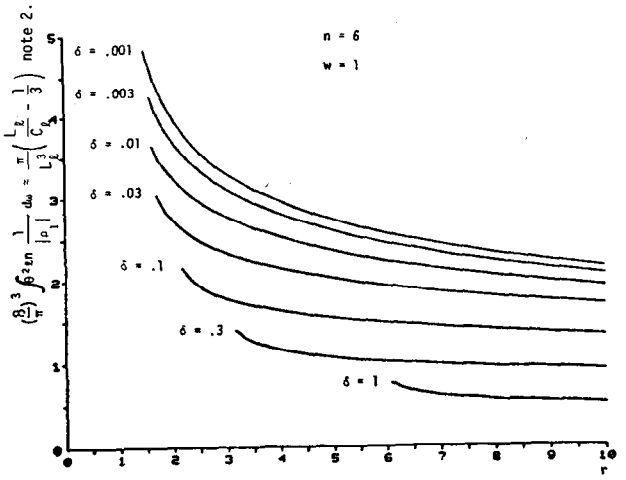

Fig. 30. Distributed network integral restrictions.

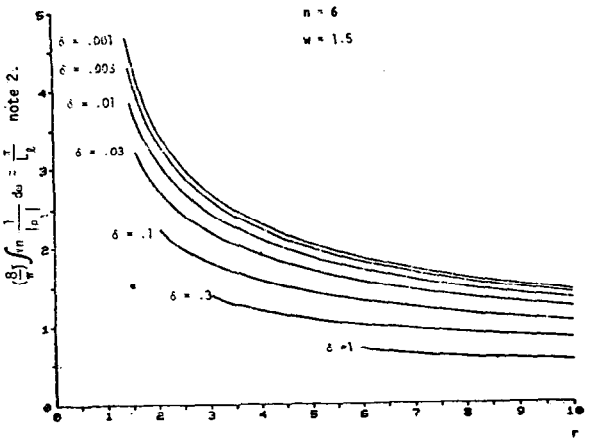

Fig. 31. Distributed network integral restrictions.

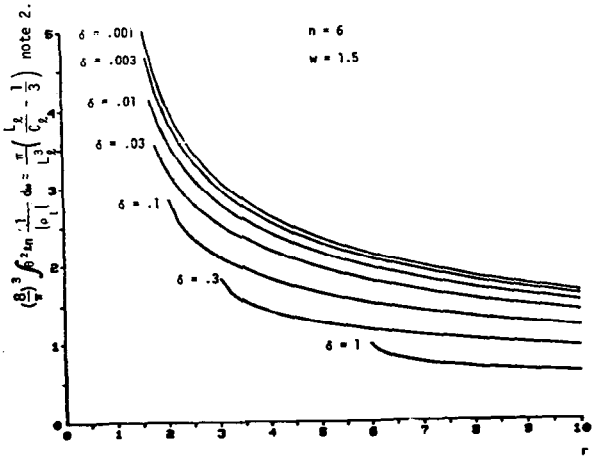

Fig. 32. Distributed network integral restrictions.

fact that $|\rho_1|^2 = 1 - |t|^2$, yields the curves shown in Figs. 21–32.

D. Numerical Example of a Practical Matching Network

As a specific problem, suppose that an amplifier is to be designed having a center frequency of 1.5 GHz and a bandwidth of at least 1 GHz. In addition, suppose that the minimum power gain within this band is to be 7 dB. The Motorola MRF901 transistor fulfills the basic requirements with an f_T of 4.5 GHz and a typical power gain of 8 dB at 2 GHz.

Before the synthesis can proceed, it is necessary to obtain suitable equivalent circuits for the input and output impedances of the transistor from the scattering parameters that are given. The output equivalent circuit so obtained is shown in Fig. 33 and the impedance is also displayed on a Smith chart in Fig. 34 for comparison with the original S-parameters. It seems worthwhile to mention here that the S-parameters used were in fact a modified set of S-parameters obtained by taking into account the emitter lead inductance. Having derived suitable equivalent circuits, the next step is to determine the parameters characterizing the frequency response.

The relative bandwidth is $w=(2.0-1.0)/1.5=0.667$. However, to provide some margin for error, let $w=1$. The normalized lower and upper band edges from (21) and (22) are then

$$\theta_a=\frac{\pi}{8}\left(1-\frac{1}{2}\right)=0.196350 \text{ rad}$$

and

$$\theta_b=\frac{\pi}{8}\left(1+\frac{1}{2}\right)=0.589049 \text{ rad.}$$

Substitution of these values into (24) yields

$$\theta_0=0.429443 \text{ rad}$$

and subsequent substitution into (23) yields

$$A=6.10973.$$

To prevent loss of accuracy, the preceding numbers will not be rounded off at this point, since later in the synthesis it will be required to subtract numbers nearly equal in value.

The next step is to choose the transfer function parameters consistent with the integral restrictions. In the calculations to follow, the output equivalent circuit for the transistor has arbitrarily been used to illustrate the procedure, with only the results for the input circuit being given at the end of this section.

Substituting into (28a) and (28b) the values from the output equivalent circuit of Fig. 33(b) yields

$$\left(\frac{8}{\pi}\right)\int_0^{\pi/2} \ln \frac{1}{|\rho_1(\theta)|}\, d\theta=\frac{\pi}{0.891198}=3.53 \quad (29a)$$

$$\left(\frac{8}{\pi}\right)^3\int_0^{\pi/2} \theta^2 \ln \frac{1}{|\rho_1(\theta)|}\, d\theta=\frac{\pi}{(0.891198)^3} \cdot\left(\frac{0.891198}{0.0684215}-\frac{1}{3}\right)=56.3. \quad (29b)$$

Referring to the integral curves of Figs. 29 and 30, the value of 3.53 for the integral at $r=2.67$ falls outside the

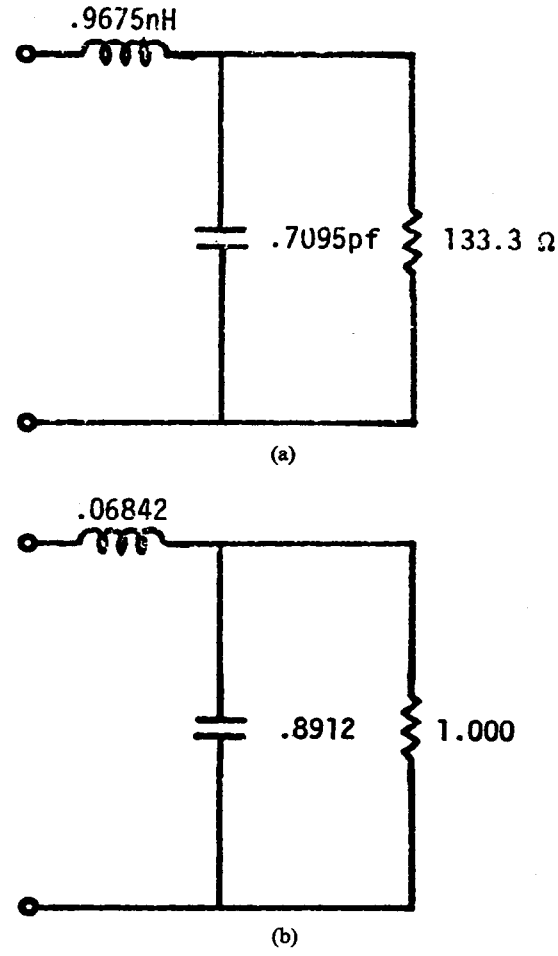

Fig. 33. Transistor output equivalent circuit.

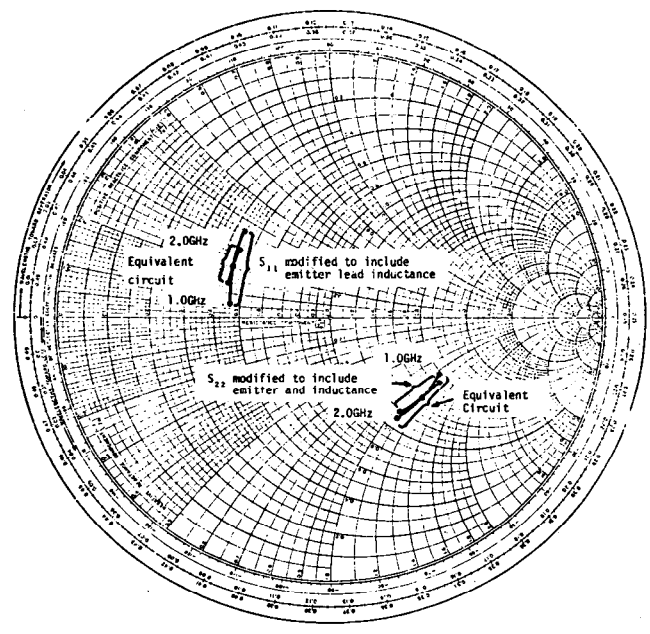

Fig. 34. Transistor equivalent circuit impedances.

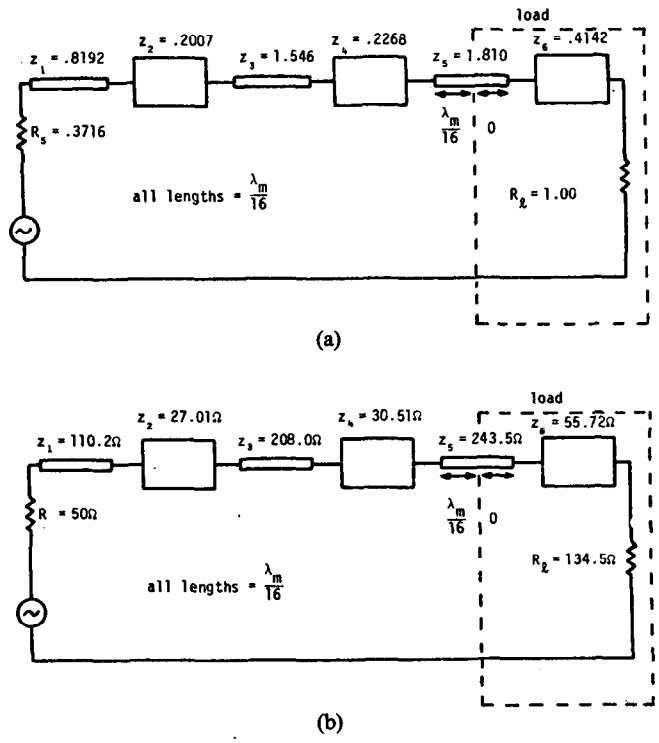

Fig. 35. Synthesized transistor output matching network. (a) Normalized. (b) Denormalized.

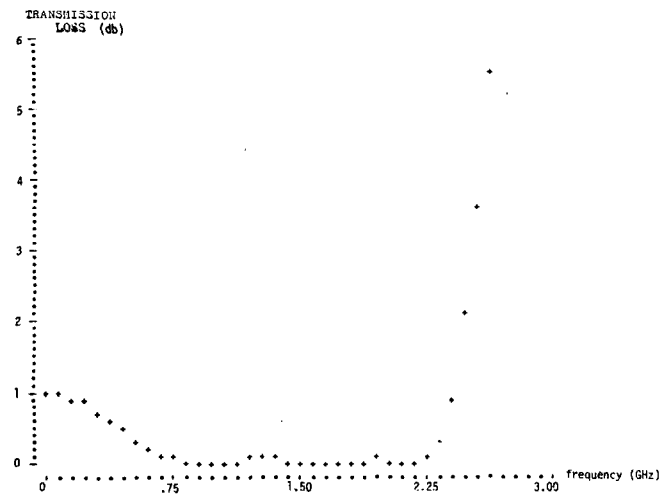

Fig. 36. Computer analysis plot of synthesized transistor output circuit.

range of the curves. Normally n is chosen on the basis of maximum attenuation in the passband. However, in this case by choosing $n=6$, a value for δ can be obtained by extrapolation from Fig. 29 as

$$\delta = 0.00045.$$

Turning now to Fig. 30, for $r=2.67$ and $\delta=0.00045$, the second integral's value is real as 3.57, well below the upper limit of 56.3 set by (29b), and thus the second integral restriction is satisfied. Having chosen δ, ϵ can now be found using the equation

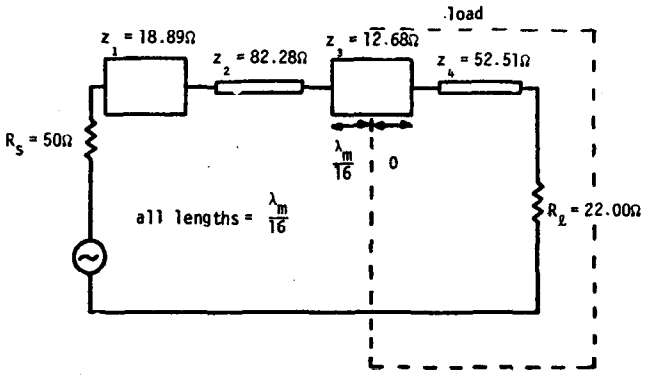

Fig. 37. Synthesized transistor input matching network.

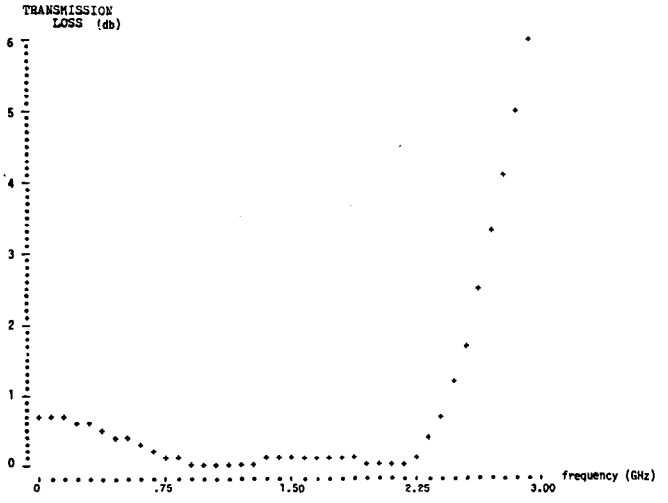

Fig. 38. Computer analysis plot of synthesized transistor input circuit.

$$\epsilon = \frac{\frac{(r+1)^2}{4r} - 1 - \delta}{\cosh^2\left[\frac{n}{2}\cosh^{-1}(A\omega_0^2)\right]}.$$

Substituting $r=2.67$, $n=6$, $\delta=0.00045$, and $\omega_0=0.457947$ gives $\epsilon=0.0124326$. The expected frequency response with these parameters substituted into (26) is shown in Fig. 20. The maximum insertion loss in the passband is then

$$L_{A\,\max} = 10\log(1+\delta+\epsilon) = 0.0556 \text{ dB}.$$

The synthesis procedure which can now begin is entirely similar to that already carried out for the lumped element synthesis of Section III, except for the final transmission line extractions. For this reason only results for the important stages of the procedure will be included. As for the lumped element case, the low-pass prototype poles and zeros are computed from (11) as

$$p'_{pi} = \pm 1.11949 + j0,\ \pm 0.559745 \pm j1.29998$$

and

$$p'_{0i} = \pm 0.063081 + j0,\ \pm 0.031541 \pm j0.867747$$

ρ_1 for the mapped response, including the factor K from

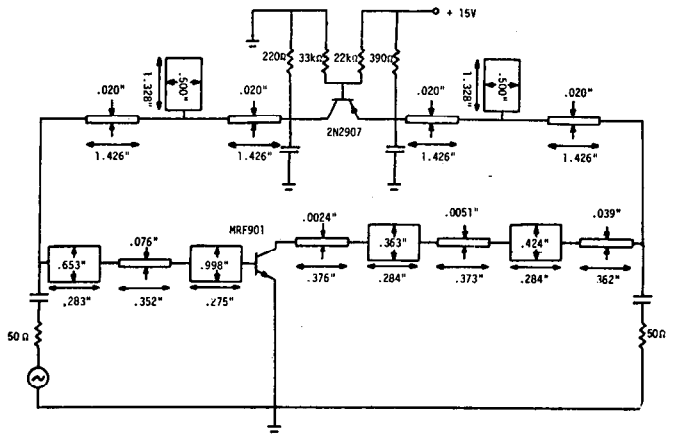

Fig. 39. Experimental circuit.

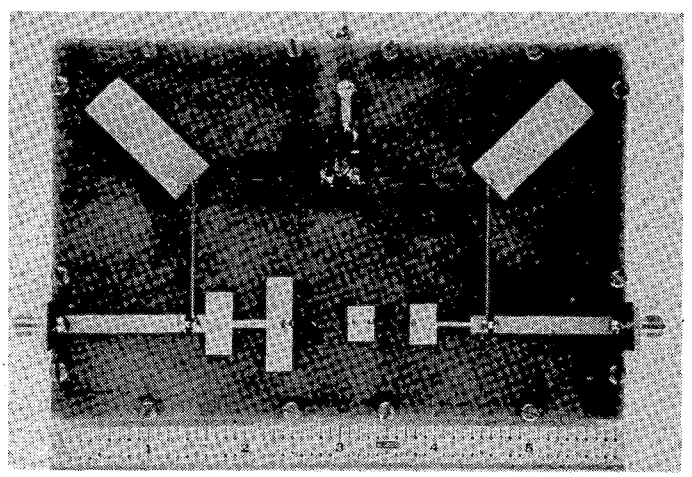

Fig. 40. Transistor amplifier.

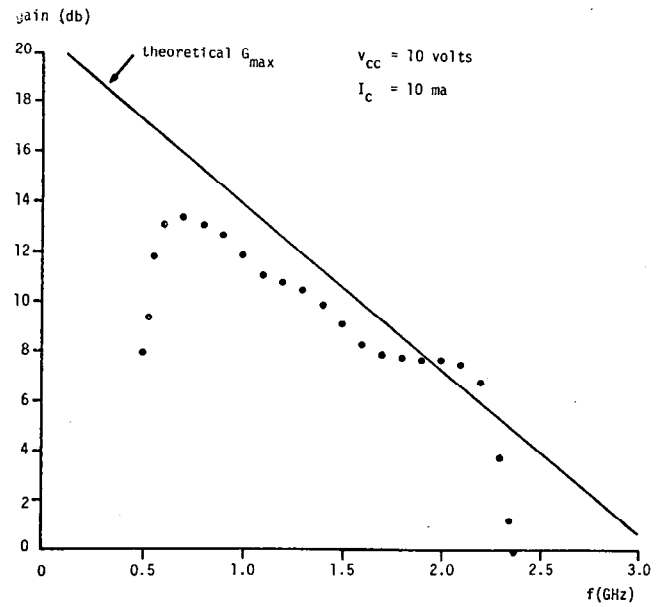

Fig. 41. Measured transistor amplifier frequency response.

the circuit of Fig. 35(b). A computer generated network analysis program was run on this circuit and the resulting frequency response plot is shown in Fig. 36. Comparison of this figure with the original transfer function plot of Fig. 20 shows excellent agreement.

The development of a suitable matching network for the input of the transistor follows an entirely similar procedure and the results are as follows. With $n=4$, $r=0.44$, and $w=1$, δ was chosen as $\delta=0.001$, resulting in $\epsilon=0.0340$. The calculated maximum attenuation in the passband was then $L_{A\,\max}=0.149$ dB. The resultant circuit and computer analyzed frequency response are shown in Figs. 37 and 38. The next section develops and gives experimental results for a physical circuit based on the calculations of this section.

(25), is then computed using (27) as

$$\rho_1(p)=\frac{0.99995p^6+0.0601696p^5+0.680529p^4+0.0285615p^3+0.123225p^2+0.00252180p+0.00511673}{p^6+1.10594p^5+1.28994p^4+0.747056p^3+0.348047p^2+0.0847835p+0.0112615}$$

and the impedance $Z(p)=(1-\rho_1)/(1+\rho_1)$ then follows immediately as

$$z(p)=\frac{0.0000503063p^6+1.04577p^5+0.609408p^4+0.718494p^3+0.224822p^2+0.0822617p+0.00614475}{1.99995p^6+1.16611p^5+1.97047p^4+0.775617p^3+0.471273p^2+0.0873053p+0.0163782}.$$

The transmission line elements are now extracted using the procedure described by Richards [12], yielding the following line impedances and termination:

$$z_6=0.4142$$
$$z_5=1.80979$$
$$z_4=0.226797$$
$$z_3=1.54616$$
$$z_2=0.200742$$
$$z_1=0.819157$$

and

$$R_0=0.371649.$$

Denormalizing and scaling $(x(1)/(0.371649))$ so as to make the normalized source resistance equal to 1, yields

V. Experimental Development and Results

An actual amplifier based on the previous calculations of Section IV was constructed. A circuit diagram and a photograph of the amplifier are shown in Figs. 39 and 40. The circuit was constructed in microstrip with dimensions calculated from charts available in the literature [13] and [14]. The measured frequency response of this amplifier is shown in Fig. 41 and is seen to be in good agreement with the maximum available gain $G_{\max}$ of the transistor obtained from the data sheets. It is worth noting that, in

contrast to designs with a flat response, the design here makes maximum use of the available gain of the transistor over the whole passband which exhibits an approximately 6-dB per octave rolloff. For designs requiring a flat response, one is referred to a paper by Ku and Peterson [15], where computer optimized element values are tabulated.

VI. Conclusion

In this paper procedures for the synthesis of lumped and distributed ladder type matching networks have been presented, based on fundamental gain-bandwidth integral restrictions derived by Fano [1]. Heretofore, synthesis procedures based on these restrictions have not found wide application due to computational difficulties. In this paper these difficulties have been avoided by numerically evaluating the appropriate integrals and using the results so obtained (in graphical form) as the basis for the synthesis of suitable matching networks. Both the lumped and distributed synthesis procedures are fully illustrated with worked examples including experimental results for a broadband microwave transistor amplifier based on the distributed example.

References

[1] R. M. Fano, "Theoretical limitations on the broadband matching of arbitrary impedances," *J. Franklin Inst.*, vol. 249, pp. 57–83, Jan. 1950; and pp. 139–155, Feb. 1950.

[2] H. W. Bode, *Network Analysis and Feedback Amplifier Design*. New York: Van Nostrand, 1945.

[3] D. C. Youla, "A new theory of broad-band matching," *IEEE Trans. Circuit Theory*, vol. CT-11, pp. 30–50, Mar. 1964.

[4] Y. T. Chan and E. S. Kuh, "A general matching theory and its application to tunnel diode amplifiers," *IEEE Trans. Circuit Theory*, vol. CT-13, pp. 6–18, Mar. 1966.

[5] H. J. Carlin, "Synthesis techniques for gain-bandwidth optimization in passive transducers," *Proc. I.R.E.*, vol. 48, Oct. 1960.

[6] R. Levy, "Explicit formulas for Chebyshev impedance-matching networks, filters, and interstages," *Proc. IEEE*, vol. 53, pp. 939–963, Aug. 1964.

[7] D. C. Fielder, "Broad-band matching between load and source systems," *I.R.E. Trans. on Circuit Theory*, vol. CT-8, pp. 138–153, June 1961.

[8] R. S. Tucker, "Gain-bandwidth limitations of microwave transistor amplifiers," *IEEE Trans. Microwave Theory Tech.*, vol. MTT-21, pp. 322–327, May 1973.

[9] O. Pitzalis, Jr., and R. A. Gilson, "Broad-band microwave class-*C* transistor amplifiers," *IEEE Trans. Microwave Theory Tech.*, vol. MTT-21, pp. 660–668, Nov. 1973.

[10] G. L. Matthaei, "Tables of Chebyshev impedance—transforming networks of low-pass filter form," *Proc. IEEE*, vol. 52, pp. 939–963, Aug. 1964.

[11] ——, "Short-step Chebyshev impedance transformers," *IEEE Trans. Microwave Theory Tech.*, vol. MTT-14, pp. 372–383, Aug. 1966.

[12] P. I. Richards, "Resistor-transmission-line circuits," *Proc. I.R.E.*, vol. 36, pp. 217–220, Feb. 1948.

[13] *Microwave J. Int.*, Feb. 1969 (Microwave Engineers Technical and Buyers Guide Edition.)

[14] P. Silvester and P. Benedek, "Equivalent capacitances of microstrip open circuits," *IEEE Trans. Microwave Theory Tech.*, vol. MTT-20, Aug. 1972.

[15] W. H. Ku and W. C. Petersen, "Optimum gain-bandwidth limitations of transistor amplifiers as reactively constrained active two-port networks," *IEEE Trans. Circuits Syst.*, vol. CAS-22, pp. 523–533, June 1975.

Robert M. Cottee was born in Sydney, Australia, on June 6, 1945. He received the B.Sc. and B.E. degrees from the University of Sydney, in 1966 and 1968, respectively. He also received the M.S. degree at Duke University, Durham, NC.

In 1968, he joined the Australian Government Department of Civil Aviation and worked on ground-based navigational aids for aircraft. From 1969 to 1973 he was with Standard Telephones and Cables Pty. Ltd., Sydney. During 1974 he was with I.T.T. Telecommunications, Raleigh, NC, where he was engaged in development of microwave communication links. He is now with the Data Systems Group of Amagamated Wireless (Australasia) Ltd.

William T. Joines (M'61) was born in Granite Falls, NC, on November 20, 1931. He received the B.S.E.E. degree with high honors from North Carolina State University, Raleigh, in 1959, and the M.S. and Ph.D. degrees in electrical engineering from Duke University, Durham, NC, in 1961 and 1964, respectively.

From 1959 to 1966, he was a Member of the Technical Staff at Bell Telephone Laboratories, Winston-Salem, NC, where he was engaged in research and development of microwave components and systems for military applications. He joined the Faculty of Duke University in 1966, and is currently an Associate Professor of Electrical Engineering. His research and teaching interests are in the area of electromagnetic wave interactions with materials. He has published numerous papers in this area.